JOURNAL OF GEOPHYSICAL RESEARCH, VOL. 104, NO. C4, PAGES 7667–7681, APRIL 15, 1999

A third-generation wave model for coastal regions
2. Verification

R. C. Ris,[1] L. H. Holthuijsen, and N. Booij
Delft University of Technology, Faculty of Civil Engineering, Delft, Netherlands

Abstract. A third-generation spectral wave model (Simulating Waves Nearshore (SWAN)) for small-scale, coastal regions with shallow water, (barrier) islands, tidal flats, local wind, and ambient currents is verified in stationary mode with measurements in five real field cases. These verification cases represent an increasing complexity in two-dimensional bathymetry and added presence of currents. In the most complex of these cases, the waves propagate through a tidal gap between two barrier islands into a bathymetry of channels and shoals with tidal currents where the waves are regenerated by a local wind. The wave fields were highly variable with up to 3 orders of magnitude difference in energy scale in individual cases. The model accounts for shoaling, refraction, generation by wind, whitecapping, triad and quadruplet wave-wave interactions, and bottom and depth-induced wave breaking. The effect of alternative formulations of these processes is shown. In all cases a relatively large number of wave observations is available, including observations of wave directions. The average rms error in the computed significant wave height and mean wave period is 0.30 m and 0.7 s, respectively, which is 10% of the incident values for both.

1. Introduction

The wave model Simulating Waves Nearshore (SWAN) has been developed by the authors (described by *Booij et al.* [this issue]) to estimate wave conditions in small-scale, coastal regions with shallow water, (barrier) islands, tidal flats, local wind, and ambient currents. It is a third-generation, discrete spectral wave model that describes the evolution of the two-dimensional wave energy spectrum in arbitrary conditions of wind, currents, and bathymetry. It assembles all relevant processes of generation, dissipation, and nonlinear wave-wave interactions in a numerical code that is efficient for small scale, high-resolution applications. The model is a synthesis of state-of-the-art formulations, but many questions are still open, and significant improvements may be expected in the future. In this study, SWAN is verified in five rather complex field cases from the southern North Sea coast. In these cases the residence time of the waves in the area is small compared to the timescale of the variation of the external conditions, so that the stationary mode of SWAN is used.

The results of the SWAN computations are presented and compared with the observed significant wave height, mean wave period, and mean wave direction. In addition, a comparison is made between computed and observed spectra. The structure of the paper is as follows. The SWAN model is briefly described in section 2. The verification cases are described in section 3. A quantitative analysis of these verifications is given in section 4. A discussion and the conclusions of this study are given in sections 5 and 6, respectively.

[1]Now at WL/Delft Hydraulics, Delft, Netherlands.

Paper number 1998JC900123.
0148-0227/99/1998JC900123$09.00

2. SWAN Model

The basic equation that is used in the SWAN model is the action balance equation [e.g., *Hasselmann et al.*, 1973]:

$$\frac{\partial}{\partial t} N + \frac{\partial}{\partial x} c_x N + \frac{\partial}{\partial y} c_y N + \frac{\partial}{\partial \sigma} c_\sigma N + \frac{\partial}{\partial \theta} c_\theta N = \frac{S}{\sigma} \qquad (1)$$

in which $N(\sigma, \theta; x, y, t)$ is the action density as a function of intrinsic frequency σ, direction θ, horizontal coordinates x and y, and time t. The first term on the left-hand side represents the local rate of change of action density in time, the second and third terms represent propagation of action in geographical x, y space, respectively (with propagation velocities c_x and c_y). The fourth term represents shifting of the relative frequency due to variations in depths and currents (with propagation velocity c_σ in σ space). The fifth term represents depth- and current-induced refraction (with propagation velocity c_θ in θ space). The expressions for these propagation speeds are taken from linear wave theory [e.g., *Whitham*, 1974; *Dingemans*, 1997]. Note that diffraction is not included in the model. The term S [$= S(\sigma, \theta; x, y, t)$] at the right-hand side of the action balance equation is a source term representing the effects of generation, dissipation, and nonlinear wave-wave interactions. The formulations of these processes in deep and intermediate-depth water in the present study are those that performed best in the validation and verification study of *Booij et al.* [this issue, Table 1]: for wind input and whitecapping the expressions of *Komen et al.* [1984] are used, for quadruplet wave-wave interactions those of *Hasselmann et al.* [1985] are used, and for bottom friction, those of *Hasselmann et al.* [1973] (Joint North Sea Wave Project (JONSWAP)) are used. This set of formulations is identical to the one that is used in cycle 3 of the Wave Model (WAM) [*the WAMDI Group*, 1988]. For triad wave-wave interactions the expression of *Eldeberky* [1996] is used, and for depth-induced wave breaking a spectral version of the model of *Battjes and Janssen* [1978]. Alternative formulations for these [*Booij et al.*, this issue, Table 1] will be con-

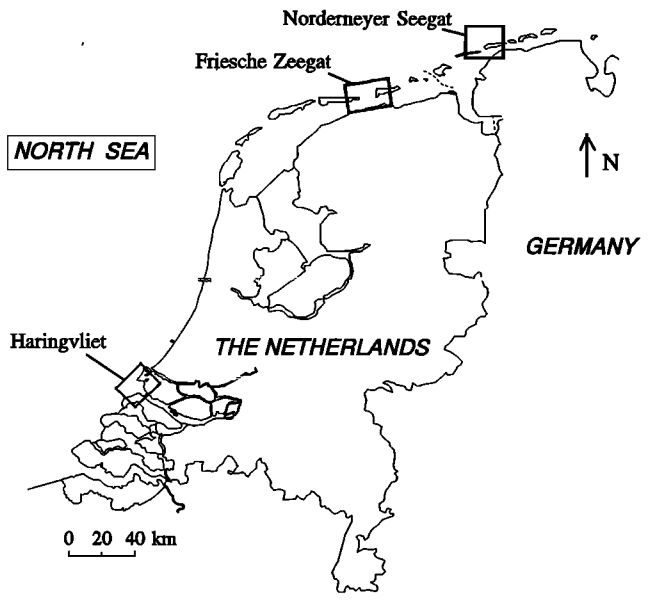

Figure 1. Locations of the three field cases along the Dutch and German coasts in the southern North Sea.

sidered later. The numerical scheme of the model is also described by *Booij et al.* [this issue]. In geographic space it is a first-order upwind scheme. In spectral space (refraction and frequency shifting) a mixed upwind/central scheme is chosen for this study ($\mu = \nu = 1/2$, [*Booij et al.*, this issue, equation (6)].

3. Verification Cases

The cases that are used for verification are from the Haringvliet, the Norderneyer Seegat, and the Friesche Zeegat in Netherlands and Germany (see Figure 1). They represent an increasing complexity in two-dimensional bathymetry and added presence of currents. In the two most complex cases (from the Friesche Zeegat) the waves propagate through a tidal gap between two barrier islands into a bathymetry of channels and shoals with tidal currents where the waves are regenerated by a local wind. In all cases a relatively large number of wave observations is available, including observations of wave directions. The computations are carried out iteratively to account for interaction between the four directional quadrants of the spectrum [see *Booij et al.*, this issue, section 3.2]. The iteration is terminated when the change (from one iteration to the next) in significant wave height H_s [$= 4(m_0)^{1/2}$, where $m_n = \int \sigma^n E(\sigma)\, d\sigma$) and $E(\sigma)$ is the variance density spectrum] in more than 97% of the submerged grid points is less than 3% or 0.03 m and also the change in intrinsic mean wave period T_{m01}[$= 2\pi\, m_0/m_1^{1/2}$] is less than 3% or 0.3 s.

In the computations of each case the upwave boundary of the wave model is a straight line, through a deepwater observation station and roughly parallel to the local depth contour. The incident wave conditions along this upwave boundary are assumed to be uniform, given by the observed frequency spectrum at that station with a $\cos^m(\theta)$ directional distribution around the observed mean wave direction. The value of the width parameter m of this distribution is inferred from the observed directional width. This observed directional width is the standard deviation of the directional distribution defined by *Kuik et al.* [1988], per frequency (the Norderneyer Seegat cases) or averaged over all frequencies weighted with the spectral density (the Haringvliet and the Friesche Zeegat cases). The incident wave conditions and the wind speed and wind direction are given in Table 1. The size, range, and resolutions of the computational grids in geographic and spectral space that are used in the computations are given in Table 2. The travel time of the waves through each of these areas was deemed to be small compared to the time variation of wind, current, and tide, and the stationary mode of SWAN was therefore used. It was verified that all computations converged monotonously (with slight oscillations that were less than the break-off criteria). For each of the cases the physical conditions and the computations are described next and commented upon separately, both qualitatively and quantitatively. An overall quantitative analysis of the performance of SWAN in these cases is given in section 4, with a further discussion in section 5.

3.1. Haringvliet Case

With the express purpose of verifying operational shallow-water wave models, the Ministry of Transport, Public Works and Water Management in the Netherlands carried out a well-documented field campaign in the Haringvliet in 1982 [*Dingemans*, 1983, 1989; *Andorka Gal*, 1995]. The Haringvliet is a branch of the Rhine estuary in the southwest of the Netherlands that is separated from the main estuary by sluices. The bathymetry of the area and the locations of the eight observation stations are shown in Figure 2. The geographic situation can be characterized as a relatively shallow bay that penetrates a few kilometers into the coast, with no currents during the observations (the sluices were closed, and tides were low). The water depth is 4 to 6 m in the area considered (including the

Table 1. Wind Conditions and Incident Wave Conditions

	$H_{s,i}$, m	$T_{m01,i}$, s	$\bar{\theta}_{\text{wave},i}$, deg	$\sigma_{\theta,i}$, deg	U_{10}, m s^{-1}	θ_{wind}, deg
Haringvliet	3.56	6.7	306	31	14.0	300
Norderneyer Seegat						
Low tide	2.84	6.5	335	45	13.0	315
High tide	2.98	6.8	375	45	8.0	338
Friesche Zeegat						
Flood	2.24	5.6	328	31	11.5	320
Ebb	3.31	7.4	341	23	11.5	340

Variables are defined as $H_{s,i}$, incident significant wave height; $T_{m01,i}$, mean wave period; $\bar{\theta}_{\text{wave},i}$, mean wave direction; $\sigma_{\theta,i}$, directional spreading; U_{10}, wind speed; and θ_{wind}, wind direction for the verification cases of this study.

Table 2. Size, Range, and Resolution of the Computational Grids

	Haringvliet	Norderneyer Seegat	Friesche Zeegat
	Geographic Grid		
Size, km	14.7 × 22.0	11.1 × 15.2	31.0 × 18.8
Resolution, m	125 × 125	100 × 100	250 × 250
	*Spectral Grid**		
Range in f, Hz	0.052–1	0.045–1	0.052–1
Range in θ, deg		0–360	
Resolution		$\Delta f = 0.1f$, $\Delta\theta = 10°$	

Here f is spectra wave frequency; θ is spectral wave direction.
*Above the maximum frequency, an f^{-4} tail is added to the spectrum.

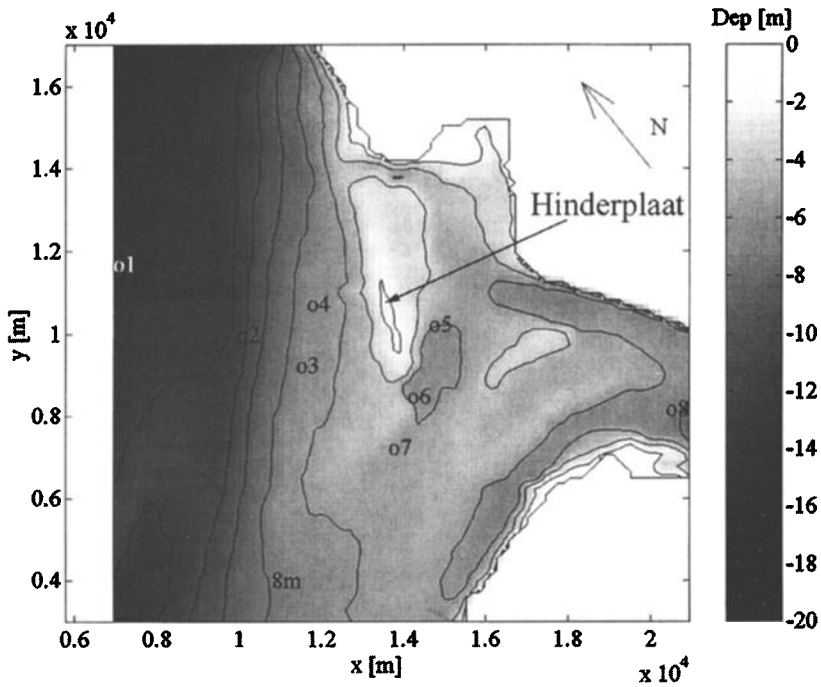

Figure 2. Bathymetry of the Haringvliet with the locations of eight observation stations (circles numbered 1 through 8).

deep water approach) and the surface area is about 10 km × 10 km. The bay is partly protected from the southern North Sea by a shoal (called the "Hinderplaat," Figure 2) of roughly 1 km × 4 km surface area, extending across half the bay entrance. The water depth over the top of the shoal during the observations was about 2 m. The waves were measured in deep water with one WAVEC pitch-and-roll buoy (station 1), six Waverider buoys scattered around the shoal (stations 2 to 7), and one wave gauge located about 5 km behind the shoal (station 8). The wind velocity, the wind direction and the water level were measured at a site near station 6.

From the extensive data set one case is selected from a local storm in the southern North Sea on October 14, 1982, which generated waves from northwesterly directions. SWAN computations are carried out at 2300 UTC on this day. This time was selected because (1) the wind speed and direction were fairly constant, (2) the waves were fairly high (for the observation period of 13 weeks), and (3) the water level was sufficiently low to see the generation of a significant secondary peak in the spectra near the shoal but not so low that the shoal would be dry. The incident wave conditions and the wind speed and direction at 2300 UTC are given in Table 1. The waves approach the estuary from deep water and break over the shoal with a reduction of significant wave height from about 3.6 m in deep water to 2.5 m just in front of the shoal to about 0.6 m just behind the shoal. The local wind regenerates the waves behind the shoal to about 1.1 m significant wave height at station 8. This large variation in significant wave height implies a large variation in the energy scale of spectra (Figure 3). The observations at the various stations were not synchronous. Therefore the two nearest observations on either side of 2300 UTC are considered at each station (Figure 6).

Figure 4 shows the pattern of the significant wave height as computed by SWAN. This pattern is consistent with the pattern of the observations: the significant wave height reduces gradually from the deepwater value of about 3.6 m to about 2.5 m in front of the shoal and then very rapidly to about 0.7 m over the shoal. South of the shoal, in slightly deeper water, the decrease of the significant wave height is more gradual. At station 8 the significant wave height has grown to about 1 m. The mean wave period (not shown here) follows roughly the same pattern. A comparison of the observed significant wave height and mean wave period is given in Figure 5. The agreement is generally reasonable (but not for H_s at station 2), although the model tends to slightly overestimate the significant wave height and to slightly underestimate the mean wave period. By deactivating refraction in the model, it was found that the effect of refraction is relatively unimportant (the rms difference is 0.05 m for the significant wave height over the entire computational region). This is typical of short-crested, random waves in small-scale coastal regions, for which the focusing and defocusing of individual wave components tend to cancel in a short-crested sea. Repeated computations with various source terms activated or deactivated have shown that the initial gradual decrease of wave height is caused by bottom dissipation, whereas the subsequent rapid decrease over the shoal is caused by depth-induced breaking. The slow increase of wave height behind the shoal is almost entirely due to regeneration by wind (and the parallel processes of whitecapping and quadruplet wave-wave interactions).

The computed spectra are compared with the observed spectra around 2300 UTC in Figure 6. The agreement is reasonable, particularly if allowance is made for the large variation in scale of the spectra (e.g., station 5 with a twentyfold change in energy scale compared to station 1). Nevertheless, the decay of the primary peak and the regeneration of high-frequency energy are overpredicted. It was verified with repeated computations that water level variations during the residence period of the waves cannot explain these discrepancies at the low-frequency peak. However, it must be stressed that only small

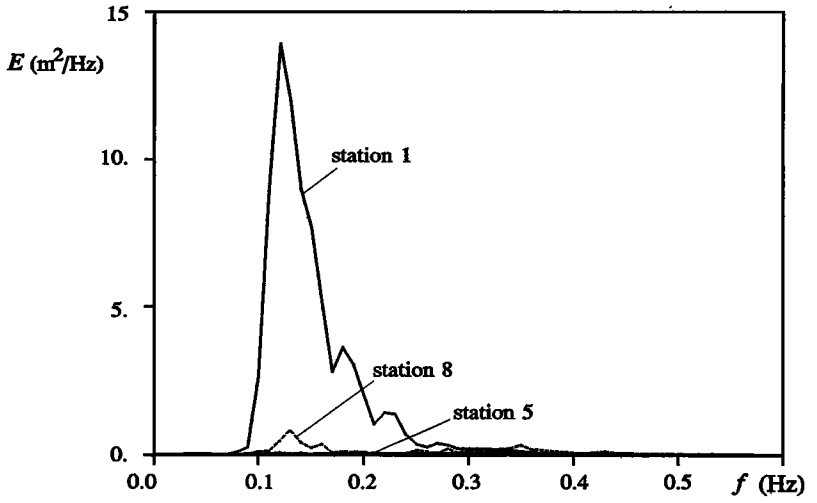

Figure 3. Observed spectra at stations 1, 5, and 8 in the Haringvliet on October 14, 1982, around 2300 UTC. Note the large difference in energy scale.

residuals of low-frequency energy are compared here. For instance, the observed reduction of the peak level between stations 1 and 8 (where the discrepancy is largest) is about 95%, whereas the computed reduction is 97%. The regeneration at high frequencies may be due to too much energy transfer from the lower frequencies by triad wave-wave interactions or by too much generation by wind. Repeated computations without triad wave-wave interactions but with wind and vice versa show that both processes are equally responsible for this high-frequency regeneration. In the other verification cases (see below) a similar phenomenon of overpredicting the regeneration of high-frequency energy occurs. Again, it must be stressed that only small numbers are involved (the computed regeneration by wind between station 5 and station 8 is only about 0.2 m). The errors at the low-frequency side of the spectrum and at the high-frequency side compensate roughly to produce a reasonably correct significant wave height, but they are the main cause for underpredicting the mean wave period.

3.2. Norderneyer Seegat Cases

The cases of the Norderneyer Seegat (Figure 7) are more complex than the Haringvliet case. This seegat is a tidal gap between the barrier islands of Juist and Norderney in the range of West Friesian Islands in the northern part of Germany. The region behind this gap is an intertidal area with shoals and channels over a distance of 7.5 km to the mainland. The main channel (16 m maximum depth) penetrates deep around the

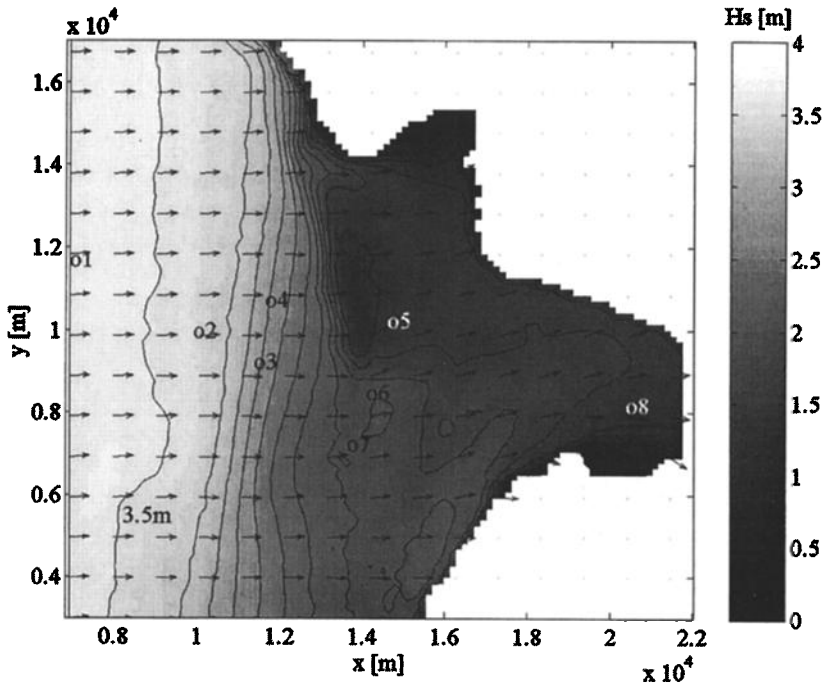

Figure 4. Computed pattern of the significant wave height and mean wave direction (unit vectors) in the Haringvliet at 2300 UTC on October 14, 1982.

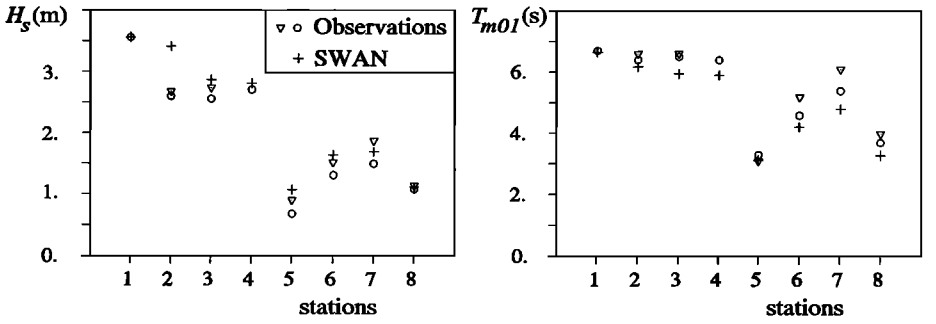

Figure 5. Observed and computed significant wave height H_s and mean wave period T_{m01} in the Haringvliet at 2300 UTC on October 14, 1982.

head of Norderney toward the east. Two smaller channels bifurcate from the western side of the Norderneyer Seegat toward the south and west. The Coastal Research Station of the Niedersächsisches Landesamt für Ökologie in Norderney carried out a rather detailed field measurement campaign in the winter of 1995–1996 with nine Waverider buoys (Figure 7), four of which were directional buoys. From the extensive data set, two typical cases have been selected: a low-tide case (November 16, 1995, 2200 UTC) and a high-tide case (November 17, 1995, 0400 UTC). The reasons that these times were selected are that (1) seven of the nine buoys were operating simultaneously (thus avoiding synchronization problems), (2) the significant wave height was relatively high, and (3) the incident frequency spectrum was unimodal. Since no current observations were available, a situation at the turn of the tide has been selected so that the effect of currents can be and has been ignored. The wind velocity and wind direction were recorded at a site located at the northern coast of Norderney (near station 2). The water levels were recorded at a tide gauge at the Norderneyer Riffgat (just south of Norderney). The

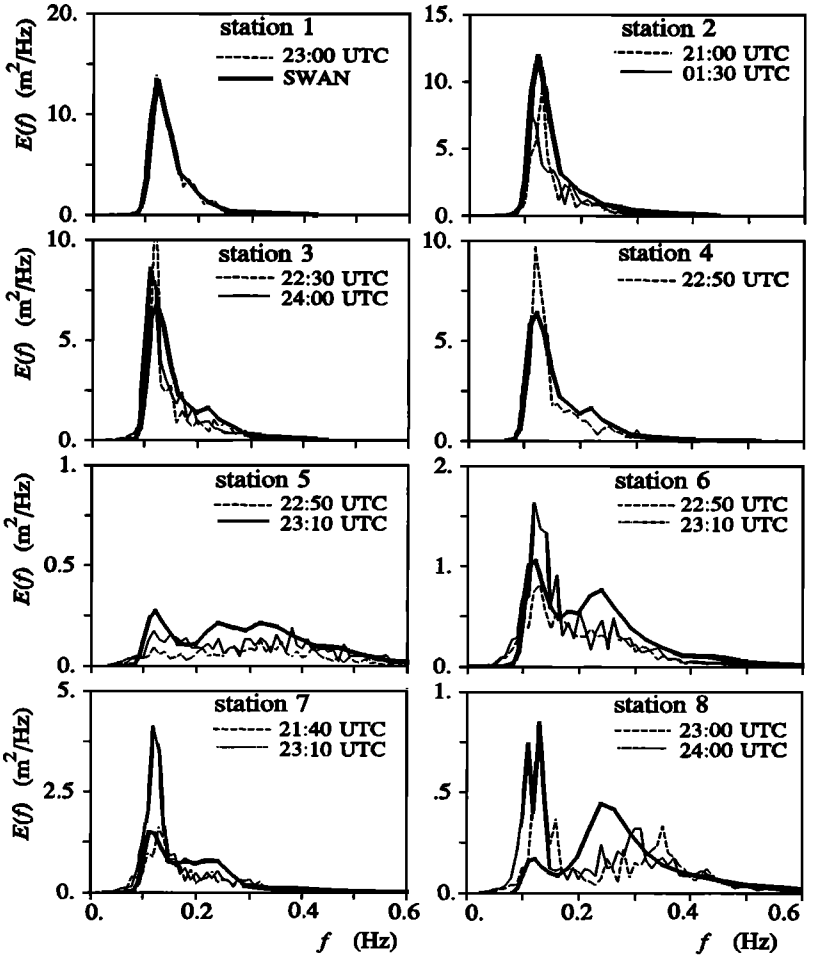

Figure 6. Observed and computed spectra in the Haringvliet on October 14, 1982 (computations at 2300 UTC and observations around 2300 UTC). Note the differences in energy density scales.

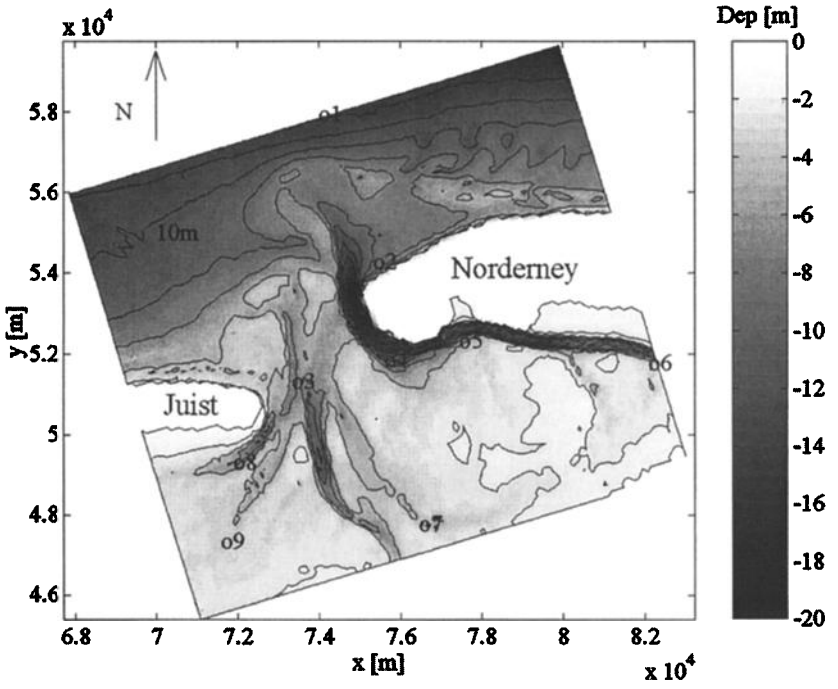

Figure 7. Bathymetry of the Norderneyer Seegat with the locations of nine observation stations (circles numbered 1 through 9).

incident wave conditions and the wind speed and direction are given in Table 1. Because no information was available on the spatial variations of the wind field and the water levels, they are assumed to be uniform over the region. As the waves propagate from deep water to the barrier islands, the wave height decreases gradually from about 3 m to about 1 m or about 2.5 m (at station 2 in the low-tide case and high-tide case, respectively). It is obvious from the observed spectra (Figure 10, low tide) that the wave conditions in the region between the islands and beyond the islands are dominated by local wind effects (the low-frequency energy at station 1 is not present at stations 4 to 9).

Figure 8 shows the pattern of the significant wave height and the mean wave direction for the low-tide case (2200 UTC) as computed by SWAN. This pattern is consistent with the pattern of the observations: the significant wave height reduces gradually from the deepwater value of about 3 m to about 1 m in front of the tidal gap. As the waves propagate through the gap, they refract out of the channels to the shallower parts where wave energy is dissipated rapidly. The local wind regenerates high-frequency waves in the interior region, in particular, in the deep channels, thus decreasing the mean wave period from 6 s at the deepwater site to about 2 s. Beyond the island of Norderney the waves completely reverse their direction owing to refraction effects.

The comparison between the computed and observed significant wave height and mean wave period is reasonable, as is evident from Figure 9. Generally, the model overestimates slightly the significant wave height and underestimates the mean wave period. The mean wave direction can be compared with observations at stations 2 and 4, where the difference is 9° and 13°, respectively. From repeated computations with and without wind it was found that the wave conditions over the tidal flats and in the channels are primarily determined by the local wind; e.g., the significant wave height at station 7 decreases from 0.39 to 0.05 m when wind is deactivated. The effect on the mean wave period is less pronounced (mean wave period at station 7 changes from 2.0 to 2.4 s when wind is turned off). A comparison between the computed and the observed spectra is shown in Figure 10. It is obvious that the spectra are not well reproduced by the model, but the 2 orders of magnitude difference in energy levels between stations 1 and 9 should be noted. These discrepancies are discussed in section 5.

For the high-tide case (0400 UTC on November 17, 1995) the computed pattern of significant wave height and mean wave direction is very similar to that of the low-tide case. It is therefore not shown here. The agreement between the computed and observed significant wave heights and mean wave periods is again reasonable (Figure 11), with the same degree of overestimating the significant wave height at the sheltered stations 4, 5, and 6 and (slightly more) underestimating the mean wave period. The computed mean wave directions at stations 2 and 4 differ 7° and 0°, respectively, from the observed mean wave directions. The comparison between the observed and computed spectra in this high-tide case is similar to that in the low-tide case. This is shown in Figure 18, which is addressed in more detail in section 5.

3.3. Friesche Zeegat Cases

The situation of the Friesche Zeegat is geographically similar to that of the Norderneyer Seegat (Figure 12), the main difference being that the intertidal area is larger and the main channel crosses to the mainland. It has been chosen because observations are available in conditions with tidal currents that have been computed with a fair degree of detail (maximum speed of about 1 m s^{-1}). The Friesche Zeegat is located about 70 km west of the Norderneyer Seegat, between the islands of Ameland and Schiermonnikoog in the northern part of the Netherlands (Figure 1). The Ministry of Transport, Public

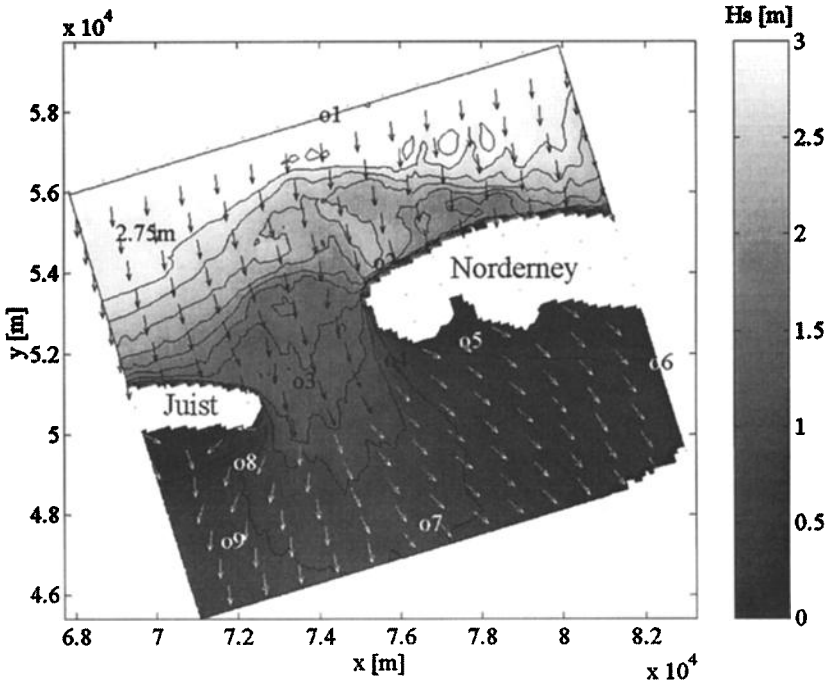

Figure 8. Computed pattern of the significant wave height and mean wave direction (unit vectors) in the Norderneyer Seegat at low tide (2200 UTC) on November 16, 1995.

Works and Water Management, Netherlands, carried out a well-documented field campaign in 1992 [e.g., *Dunsbergen*, 1995] to monitor the geophysical changes in this area after the closure of the Lauwers Zee in 1969 (bottom right corner of Figure 12). The cases that have been selected for this verification are a flood case (October 9, 1992, 0500 UTC) and an ebb case (October 9, 1992, 1100 UTC). The reasons that these times have been chosen are that (1) at these times, relatively high waves were observed (significant wave height in deep water of about 3 m); (2) during the period of the observations the wind speed was nearly constant; (3) the incident frequency spectrum was unimodal; (4) tidal currents and water levels were measured; and (5) the observations at the different stations were carried out simultaneously (thus avoiding synchronization problems). The wind velocity and direction were recorded at a station located north of Schiermonnikoog (just outside the area shown in Figure 12). The wind speed and direction, which are assumed to be uniform over the area, and the incident wave conditions are given in Table 1. The current velocities and water levels that are used in the computations have been obtained with the WAQUA circulation model [*Les*, 1996; *Stelling et al.*, 1986] and are shown for the flood case in Figure 13.

The computed pattern of the significant wave height and the mean wave direction for the flood case (October 9, 0500 UTC) is shown in Figure 14. It is consistent with the pattern of the observations: the wave height gradually decreases between the deepwater boundary and the entrance of the tidal inlet. Results of repeated computations with and without wind show that the wind generates more wave energy in the deeper eastern entrance than in the shallower western entrance of the tidal inlet (thus erroneously suggesting that the waves penetrate deeper into the eastern channel than into the western channel). After the waves travel through the tidal gap between the two barrier islands, they refract laterally to the shallower parts of the inlet. They completely reverse direction behind the two islands. The computed significant wave height and mean period at the six observation stations are given in Figure 15. The agreement

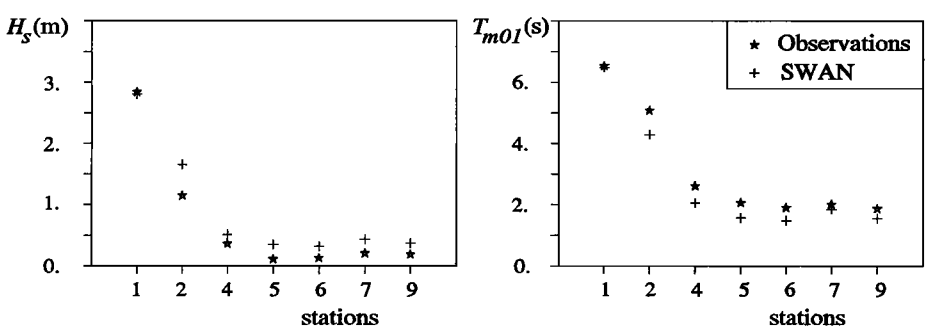

Figure 9. Observed and computed significant wave height H_s and mean wave period T_{m01} in the Norderneyer Seegat at low tide (2200 UTC) on November 16, 1995 (stations 3 and 8 missing from the data).

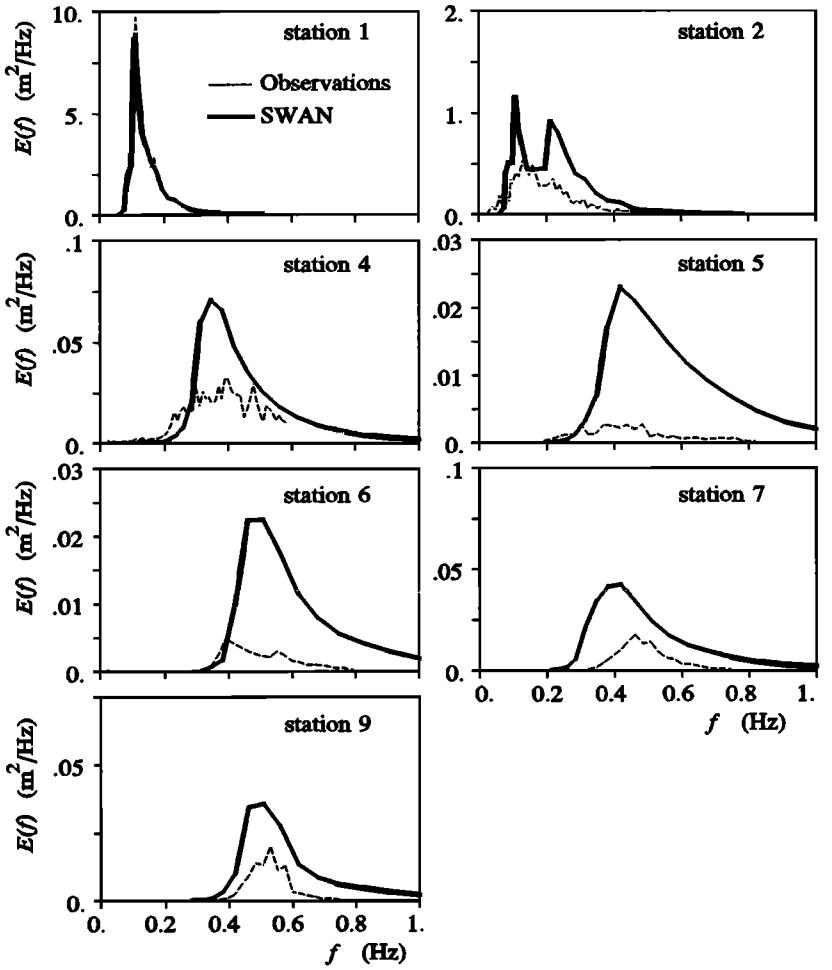

Figure 10. Observed and computed spectra in the Norderneyer Seegat at low tide (2200 UTC) on November 16, 1995. Note the differences in energy density scales.

with the observed significant wave heights is good, but the mean wave period is underestimated by approximately 1 s. The computed mean wave directions at stations 2 and 3 differ 1° and 3°, respectively, from the observed directions (but this is trivial since these stations are located seaward from the shallow area).

Computations show that the effect of the currents in the area is to decrease the significant wave height and mean wave period in the channels. For instance, at station 5 the currents reduce the significant wave height from about 0.8 m to about 0.6 m and the mean wave period from about 2.9 s to about 1.9 s. It is striking that the presence of currents in the model thus reduces the agreement with the observed mean wave period. The mean wave direction is only slightly affected by the currents (differences of about 10° at stations 4 and 5). The effect of wind is similar to that in the Norderneyer Seegat. Also, here computations show that in the model the wind is important in the inner region where waves at station 6 are regenerated (significant wave height 0.13 m without wind and 0.52 m with wind); but this regeneration is overestimated (Fig-

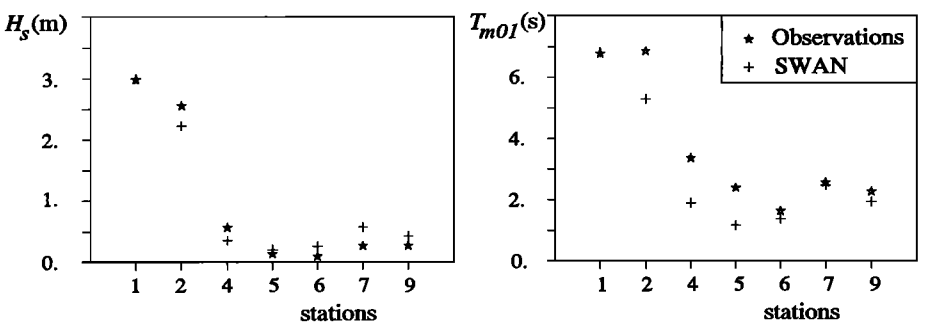

Figure 11. Observed and computed significant wave height H_s and mean wave period T_{m01} in the Norderneyer Seegat at high tide (0400 UTC) on November 17, 1995 (stations 3 and 8 missing from the data).

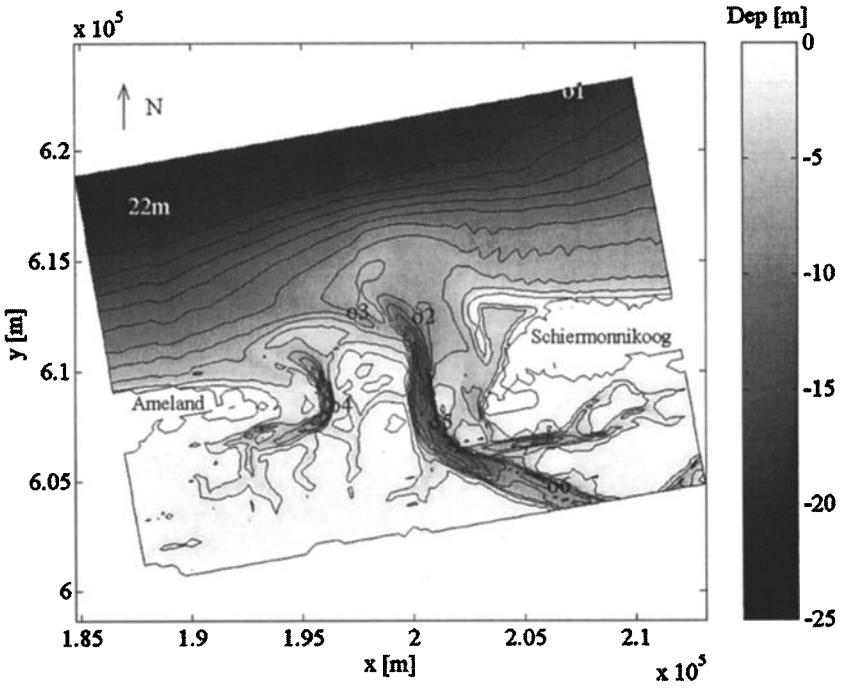

Figure 12. Bathymetry of the Friesche Zeegat with the locations of six observation stations (circles numbered 1 through 6).

ure 16), resulting in (slightly) too high significant wave heights and too low mean wave periods (Figure 15). Repeated computations with various source terms activated and deactivated show that the gradual decrease of the significant wave height north of the barrier islands and over the tidal flats is due to depth-induced wave breaking. To indicate the importance of the time variation in the observations, the observed spectra at 0600 UTC are also shown in Figure 16. It is obvious that the time variation in the observations is significant, but in view of the reasonable agreement with the observations (except at station 6) at the nominal time of the computations (0500 UTC), this time variation seems only relevant at station 6. It is also obvious that the agreement between the observed spectra and the computed spectra is better than in the case of the

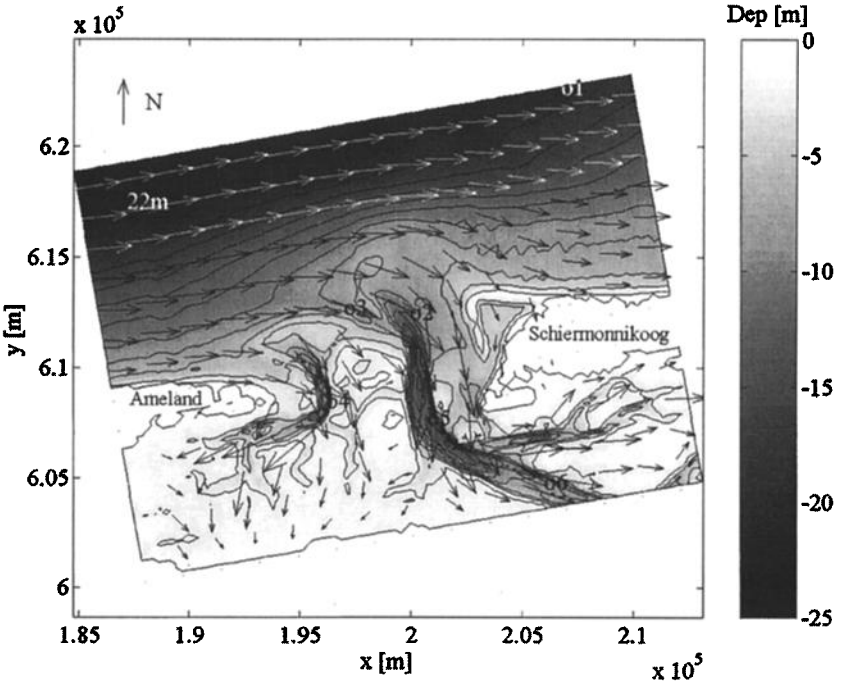

Figure 13. Water depth (storm surge added to bathymetry) and current velocity in the Friesche Zeegat during flood (0500 UTC) on October 9, 1992.

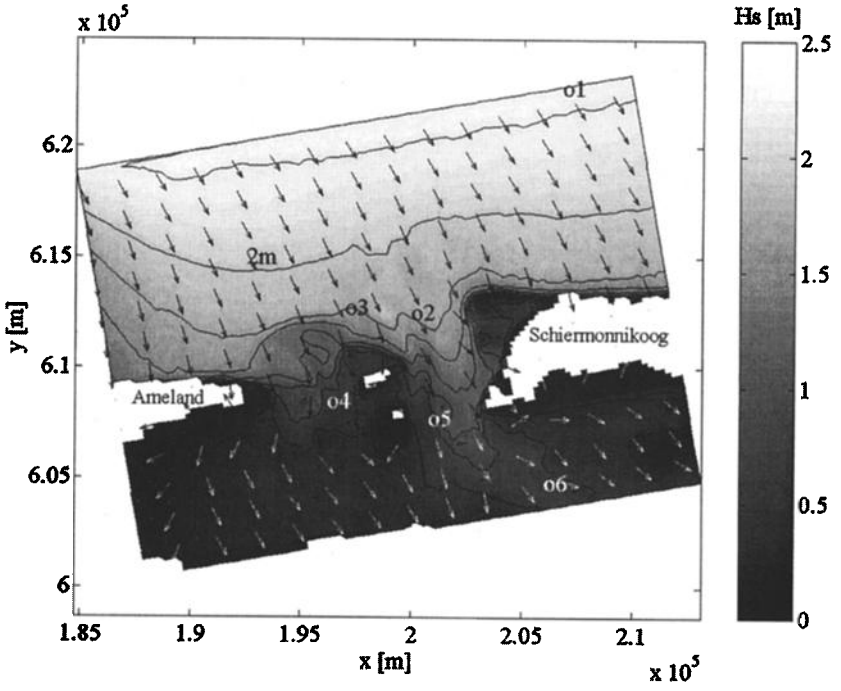

Figure 14. Computed pattern of the significant wave height and mean wave direction (unit vectors) in the Friesche Zeegat during flood (0500 UTC) on October 9, 1992.

Norderneyer Seegat (compare with Figure 10). The decay of the low-frequency peak is overpredicted (at stations 2 and 3), but the total energy involved in the relevant frequency band (0.13–0.16 Hz) is relatively small. In view of the water depth, triad wave-wave interactions seem to be relevant only at stations 2 and 3, where the high-frequency level of the computed spectra agrees well with the observed level. The overprediction of the regeneration of high-frequency energy is not as obvious as in the cases of the Haringvliet and the Norderneyer Seegat (except at station 6).

For the ebb case (October 9, 1100 UTC) the computed pattern of the significant wave height (not shown here) is similar to that of the flood case, except that the shoals in the tidal gap block wave penetration into the area (the water level is 1.25 m lower than in the flood case) and that the currents act to some extent as a waveguide (resulting in somewhat higher waves over the channels and in mean wave directions that roughly follow the pattern of the channels). The computed significant wave height and mean wave period are compared with the observed values in Figure 17. It is evident that the agreement between the observed significant wave height and the computed significant wave height is variable, whereas the computed wave periods are generally somewhat too low. The computed mean wave direction at stations 2 and 3 differ 2° and 1°, respectively, from the observed directions (but again, this is trivial as these stations are located seaward from the shallow area). The agreement between the observed and computed spectra (not shown here) is slightly better than in the flood case.

4. Model Performance

To quantify the performance of ocean wave models, a scatter index (SI) is sometimes used [e.g., *Zambreski*, 1989, 1991; see also *Komen et al.*, 1994; *Romeiser*, 1993]. It will also be used here. It is defined here as the rms error normalized with the average observed value:

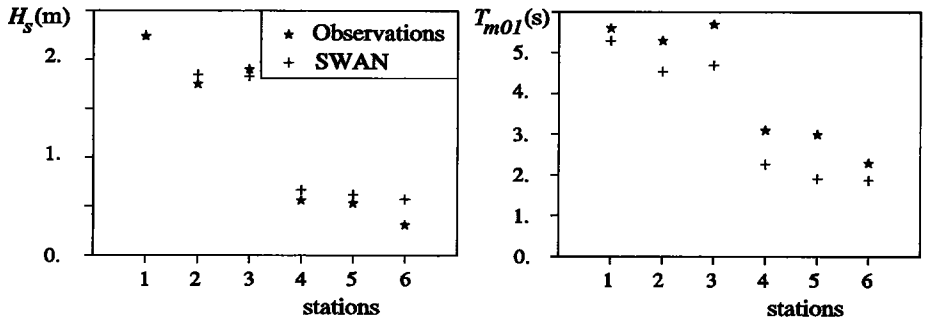

Figure 15. Observed and computed significant wave height H_s and mean wave period T_{m01} in the Friesche Zeegat during flood (0500 UTC) on October 9, 1992.

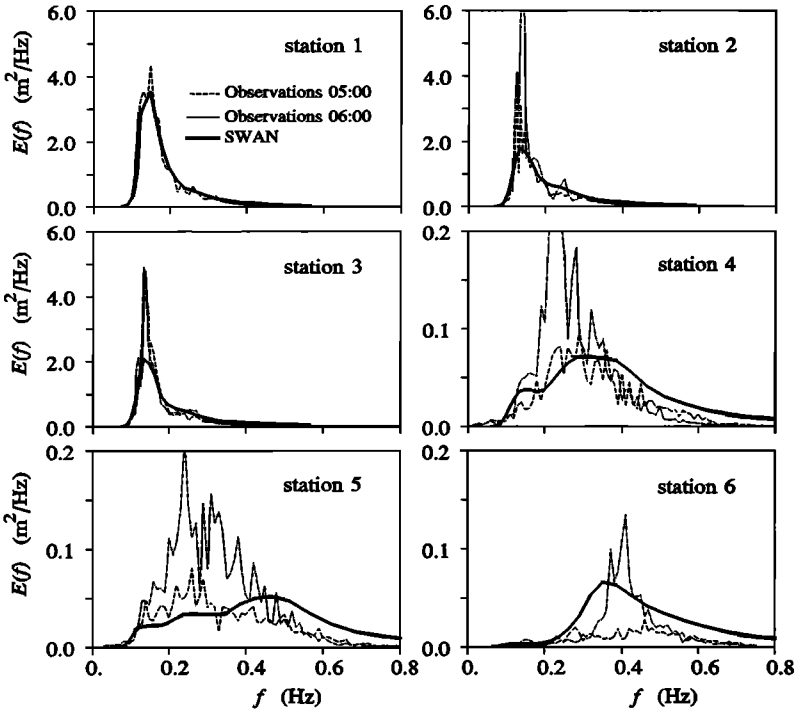

Figure 16. Observed and computed spectra for the flood case in the Friesche Zeegat on October 9, 1992. Observed at 0500 and 0600 UTC. Computed at 0500 UTC. Note the differences in energy density scales.

$$\mathrm{SI} = \frac{\mathrm{rms}_{\mathrm{error}}}{\bar{X}} \tag{2}$$

where

$$\mathrm{rms}_{\mathrm{error}} = \sqrt{\frac{1}{N}\sum_{N}(X_n - Y_n)^2} \tag{3}$$

where X_n is the observed values, Y_n is the computed values, N is the number of observations (not including the incident value), and $\bar{X}$ is the averaged observed value (not including the incident value). However, this index may appear to understate the skill of the model, as it tends to be large in coastal applications. The reason is that the rms error of the significant wave height is normalized with the average significant wave height, which is usually rather small in coastal regions. For instance, an rms error of 0.25 m in the significant wave height in complex field conditions seems reasonable, but if the mean value is only 0.5 m, the scatter index attains the rather high value of 50%.

Two alternatives are therefore considered: one to better diagnose the model performance from a modeling point of view (the model performance index (MPI)) and one that is more predictive and therefore attractive from an operational point of view (the operational performance index (OPI)). The diagnostic model performance index indicates the degree to which the model reproduces the observed changes of the waves. Like the scatter index, it is defined in terms of root-mean-square values:

$$\mathrm{MPI} = 1 - \frac{\mathrm{rms}_{\mathrm{error}}}{\mathrm{rms}_{\mathrm{changes}}} \tag{4}$$

The definition of $\mathrm{rms}_{\mathrm{changes}}$ is identical to that of $\mathrm{rms}_{\mathrm{error}}$, except that all computed Y_n values are replaced by the observed incident value X_i. For a perfect model ($\mathrm{rms}_{\mathrm{error}} = 0$) the value of the MPI would obviously be 1, whereas it would be 0 for a model that (erroneously) predicts no changes ($\mathrm{rms}_{\mathrm{error}} = \mathrm{rms}_{\mathrm{changes}}$).

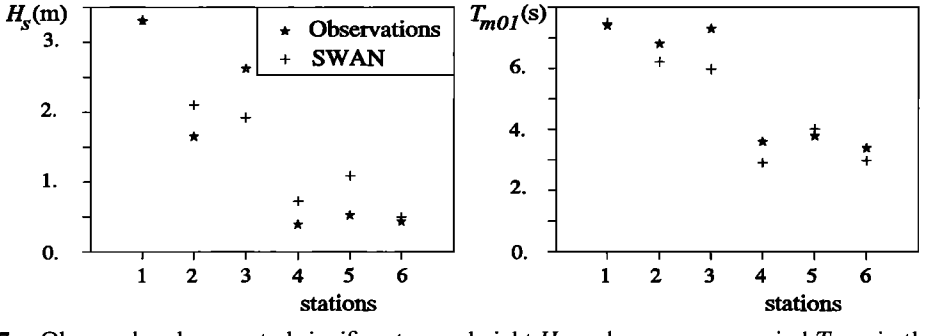

Figure 17. Observed and computed significant wave height H_s and mean wave period T_{m01} in the Friesche Zeegat during ebb (1100 UTC) on October 9, 1992.

Table 3. Performance of SWAN for the Significant Wave Height H_s

	$H_{s,i}$, m	$\bar{H}_s$, m	Bias, m	rms, m	SI	MPI	OPI
Haringvliet	3.56	1.85	0.23	0.33	0.18	0.82	0.09
Norderneyer Seegat							
Low tide	2.84	0.35	0.25	0.28	0.77	0.89	0.10
High tide	2.98	0.64	0.02	0.22	0.35	0.91	0.07
Friesche Zeegat							
Flood	2.24	1.01	0.09	0.14	0.14	0.89	0.06
Ebb	3.31	1.12	0.14	0.47	0.42	0.80	0.14
Average	2.99	0.99	0.15	0.29	0.37	0.86	0.09

Abbreviations are defined as $H_{s,i}$, incident significant wave height; $\bar{H}_s$, mean observed significant wave height; SI, scatter index (rms error, normalized with the mean of the observations); MPI, model performance index (1 minus the rms error normalized with the rms of the observed changes); and OPI, operational performance index (the rms error normalized with the incident value).

The more predictive operational performance index is defined as the rms error normalized with the incident observed value:

$$\text{OPI} = \frac{\text{rms}_{\text{error}}}{X_i} \tag{5}$$

It is predictive and operational in the sense that for a given value of the OPI (presumably a characteristic of the model and its implementation for a particular region), an error estimate can be made on the basis of incident wave conditions, prior to the computations. It does not pretend to replace the scatter index or the model performance index; it merely supplements these parameters. However, it may overstate the skill of the model for essentially the same reason that the scatter index may understate the skill of the model. Its value tends to be low because the rms error of the significant wave height is normalized with the incident significant wave height, which is usually relatively high. For instance, with an incident significant wave height of 3 m, a seemingly very reasonable OPI value of 20% is attained with a relatively large rms error of 0.6 m. To determine the systematic part of the model performance, the bias is also considered. It is simply defined as the mean error (model results minus observations, not including the incident values).

The values of these error parameters for the five cases of this study are summarized in Tables 3 and 4. These values show that, generally, SWAN performs well in these cases: the operational performance index values vary between 6% and 14% for significant wave height and between 7% and 15% for the mean wave period. The model performance index values show that, on average, the model reproduces 86% of the observed changes in significant wave height and 73% of the observed changes in mean wave period. The values of the scatter index of 37% and 20% for the significant wave height and the mean wave period, respectively, are similar to those for the WAM model in oceanic applications (e.g., *Zambreski* [1989, 1991]; see also *Komen et al.* [1994]; and *Romeiser* [1993], even if their definition is slightly different).

5. Discussion

Qualitatively, the effects of the individual processes are rather obvious. Without wind generation and the corresponding quadruplet wave-wave interactions and whitecapping, the waves behind the shoals and behind the islands would be reduced to very low, swell-type waves. Without depth-induced breaking and bottom friction the waves would be much higher, and without triad wave-wave interactions the waves would be longer. Less obvious are the effects of alternative formulations for these processes [*Booij et al.*, this issue, Table 1]. To investigate these effects, all computations have been repeated with an alternative for (1) wind growth and whitecapping (WAM cycle 3 replaced by WAM cycle 4 [*Komen et al.*, 1994], (2) bottom friction (JONSWAP replaced by *Madsen et al.* [1988]), and (3) depth-induced wave breaking (the constant value of the breaker parameter $\gamma = 0.73$ replaced by the bottom-slope-dependent value due to *Nelson* [1987], clipped as in the work by *Booij et al.* [this issue]). For the triad wave-wave interactions no alternative is available and the computations have been repeated without these interactions. The sensitivity of the model results for these alternatives are quantified for the significant wave height and the mean wave period with the rms difference and the bias relative to the above nominal results (alternative minus nominal) for the entire computed wave field and, separately, for the observations. The results of these computations (which for the observation stations are generally very similar to those of the entire wave field) are given in Table 5 (mean values per site). The biases are roughly equal to half the rms values, indicating that roughly half the variation induced by these alternative formulations contributes to increasing or decreasing the discrepancies with the observations. Generally, the effect is to slightly decrease both the significant wave height (average bias roughly 10%, bringing the results closer to the observations) and mean wave period (average bias roughly 5%, increasing the discrepancies with the observations, except the alternative wind generation, which slightly increases the mean wave period by roughly 5%). The triad wave-wave interactions do not, on average, affect the significant wave height, and they only mildly decrease the mean wave period (average bias 8%, increasing the discrepancy with the observations). On the basis of these results another set than the nominal set of formulations of the physics could be chosen to provide better agreement with the observations. However, the nominal set is based on the generic tests of the SWAN validation study [*Booij et al.*, this issue] in which the alternatives did not perform as well as the nominal set; but it must be acknowledged that the preference in these generic tests was sometimes marginal.

With the nominal formulations of the physical processes, SWAN tends to somewhat overpredict the significant wave height and to underpredict the mean wave period, mostly because of overpredicting high-frequency energy. This can be

Table 4. Performance of SWAN for the Mean Wave Period T_{m01}

	$T_{m01,i}$, s	$\bar{T}_{m01}$, s	Bias, s	rms, s	SI	MPI	OPI
Haringvliet	6.7	5.3	−0.5	0.6	0.11	0.68	0.09
Norderneyer Seegat							
Low tide	6.5	2.6	−0.4	0.5	0.19	0.88	0.07
High tide	6.8	3.2	−0.2	1.0	0.32	0.74	0.15
Friesche Zeegat							
Flood	5.6	3.9	−0.8	0.8	0.22	0.61	0.15
Ebb	7.4	5.0	−0.6	0.7	0.15	0.75	0.10
Average	6.6	4.0	−0.5	0.7	0.20	0.73	0.11

The incident mean wave period is $T_{m01,i}$, the mean observed wave period is $\bar{T}_{m01}$. SI, MPI, and OPI are defined in Table 3.

Table 5. Sensitivity of SWAN Results for Formulation of the Physical Processes

	Wind and Whitecapping, WAM 4 Versus WAM 3	Depth-Induced Breaking, *Nelson* [1987] Versus $\gamma = 0.73$	Bottom Friction, *Madsen et al.* [1988] Versus JONSWAP	Triad Interactions, No Triads Versus Triads
	Significant Wave Height H_s rms and Bias, m			
Haringvliet*	0.11 (−0.09)	0.28 (−0.22)	0.17 (−0.15)	0.07 (+0.01)
	0.11 (−0.09)	0.39 (−0.33)	0.17 (−0.06)	0.07 (−0.02)
Norderneyer Seegat*	0.17 (−0.02)	0.16 (−0.11)	0.09 (−0.07)	0.07 (−0.01)
	0.03 (−0.02)	0.14 (−0.07)	0.09 (−0.06)	0.04 (−0.02)
Friesche Zeegat*	0.07 (−0.05)	0.12 (−0.07)	0.10 (−0.07)	0.06 (+0.01)
	0.07 (−0.06)	0.12 (−0.09)	0.15 (−0.11)	0.05 (+0.03)
Average,* m	0.12 (−0.05)	0.19 (−0.13)	0.12 (−0.10)	0.06 (0.00)
	0.07 (−0.06)	0.22 (−0.16)	0.14 (−0.08)	0.05 (0.00)
Average,* %	12 (−5)	19 (−13)	12 (−10)	6 (0)
	7 (−6)	22 (−16)	14 (−8)	5 (0)
	Mean Wave Period T_m rms and Bias, s			
Haringvliet*	0.28 (+0.21)	0.25 (−0.11)	0.36 (−0.21)	0.65 (+0.45)
	0.25 (+0.19)	0.21 (−0.10)	0.27 (−0.15)	0.71 (+0.59)
Norderneyer Seegat*	0.14 (+0.12)	0.23 (−0.12)	0.32 (−0.23)	0.65 (+0.37)
	0.07 (+0.07)	0.12 (−0.06)	0.19 (−0.15)	0.51 (+0.18)
Friesche Zeegat*	0.20 (+0.17)	0.14 (−0.03)	0.30 (−0.19)	0.36 (+0.18)
	0.15 (+0.10)	0.19 (−0.13)	0.29 (−0.25)	0.33 (+0.20)
Average,* s	0.20 (+0.17)	0.21 (−0.09)	0.33 (−0.21)	0.55 (+0.33)
	0.16 (+0.12)	0.17 (−0.10)	0.25 (−0.18)	0.52 (+0.32)
Average,* %	5 (+4)	5 (−2)	8 (−5)	14 (+8)
	4 (+3)	4 (−2)	6 (−5)	13 (+8)

The root-mean-square difference and the bias (numbers in parentheses) between the computations with the nominal and alternative formulations of the physical processes [see *Booij et al.*, this issue, Table 1].

*Values in first line are for the entire computed wave field, while those in second line are for the locations of the observation stations.

well illustrated with the high-tide case of the Norderneyer Seegat (Figure 18). SWAN overestimates the high-frequency spectral levels at the sheltered stations 5 and 6 and the low-frequency spectral levels at the more exposed stations 7 and 9. It is speculated that this is due to the following three aspects.

1. High-frequency spectral levels that are too high may indicate that triad wave-wave interactions, which shift energy to these frequencies, are overestimated. However, the water depth at the stations concerned (and also some distance upwave) is not shallow, so that triad wave-wave interactions should not be effective. Computations without triad wave-wave interactions showed indeed only marginal effects at stations 5 and 6 and only some minor transfer of energy from the residual low-frequency energy to the higher frequencies at stations 7 and 9.

2. Too much regeneration by the local wind, in particular, at the sheltered stations may be due to an overestimation of the wind (at very short fetches), which was assumed to be constant and equal to the observed wind at the open sea side of the islands (and therefore overestimated). However, a computation with 30% lower wind speed (the maximum reducing effect of a developing atmospheric boundary layer from the upwind coastline to stations 5 and 6) also did not explain the discrepancies with the observations.

3. The presence of the residual low-frequency reduces the mean frequency of the waves. It would thus enhance the quadruplet interactions through the shallow-water scaling of these interactions (in the DIA approximation of *Hasselmann et al.* [1985]), and it would decrease the degree of whitecapping in the model (in the expression of *Komen et al.* [1984]). Both

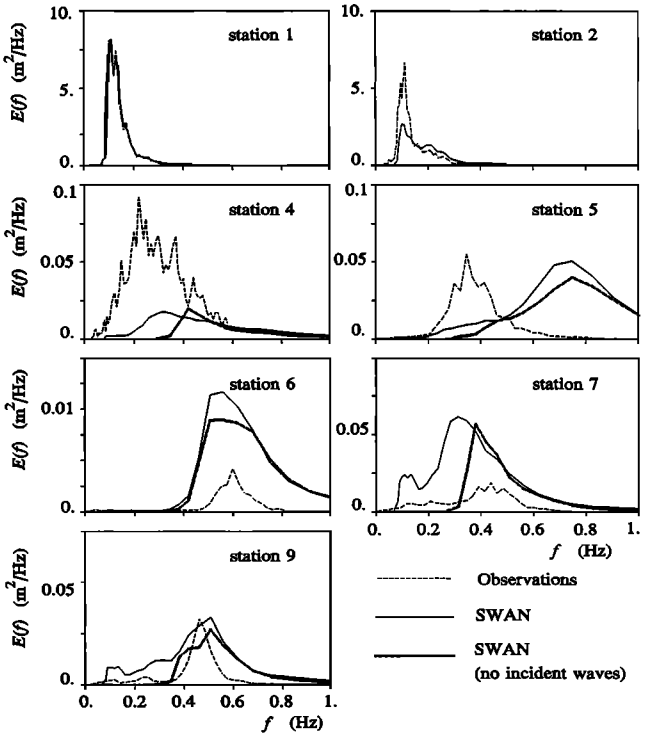

Figure 18. Observed and Computed spectra in the Norderneyer Seegat at high tide in the high-tide case (November 17, 1995, 0400 UTC). The SWAN spectra are computed with and without incident waves to show the interaction with the locally generated waves. Note the differences in energy density scales.

effects would enhance the net wave growth. To remove this residual low-frequency energy, the computation has been repeated without incident waves (resulting in local wave generation only). The results, given in Figure 18, show that indeed the presence of this residual low-frequency energy generally enhances the locally generated spectrum (at the low-frequency side). This is obvious at stations 4, 5, 7, and 9. Even at the well-sheltered station 6, where the low-frequency residual of the incident energy (frequencies less than 0.3 Hz) is less than 1% of the total energy of the spectrum, the effect is noticeable. However, whether this enhanced net wave growth is due to enhanced quadruplet wave-wave interactions or to reduced whitecapping is not clear. Moreover, the discrepancy with the observations is still large (but note the 3 orders of magnitude difference in energy scale between stations 1 and 6 and the nearly 4 orders of magnitude reduction in low-frequency energy at stations 7 and 9). A potentially larger, but equally unresolved effect (not included in the model) is the reducing effect of background low-frequency wave energy on the wave growth by wind as observed by *Donelan* [1987]. Obviously, these aspects of (re)generation of waves at short fetches in the presence of (residual) low-frequency wave energy require further investigation, but it is outside the scope of this study.

6. Conclusions

The third-generation wave model SWAN [*Booij et al.*, this issue] has been verified in stationary mode with 29 observations from 17 buoys and 1 wave gauge in five real, rather complex field cases at three sites representing an increasing complexity in two-dimensional bathymetry and added presence of currents (the Haringvliet, the Norderneyer Seegat, and the Friesche Zeegat in the Netherlands and Germany). The wave fields were highly variable with up to 3 orders of magnitude difference in energy scale in individual cases. The model accounts for shoaling, refraction, generation by wind, whitecapping, triad and quadruplet wave-wave interactions, and bottom friction and depth-induced breaking. The computations were carried out with the nominal formulations that were selected in the validation study of *Booij et al.* [this issue]. Alternative formulations for these processes in the cases considered generally increased the significant wave (10%) and mean wave period (5%). It was shown that, on average, in these cases the triad wave-wave interactions have practically no effect on the significant wave height and a mild decreasing effect on the mean wave period (8%).

Comparing SWAN results with the observations shows that with the nominal formulations of the physics, the average rms error is about 10% of the incident significant wave height and mean wave period. With these formulations, SWAN also reproduces most of the observed changes in the significant wave height and in the mean wave period (86% for the significant wave height and 73% for the mean wave period). The values of the scatter index are roughly equal to those of the WAM model in oceanic applications (37% and 20% for the significant wave height and mean wave period, respectively). In an absolute sense the rms errors are 0.30 m and 0.7 s, respectively. However, the shape of the spectrum is often not well reproduced. In particular, high-frequency growth (very short fetches) is usually overestimated. It must be noted that the observations and the model results involve a large range of wave scales within each case. This is obvious from the 1 to 3 orders of magnitude differences in spectral energy levels between deep water and the inner region. SWAN slightly overestimates this decay with 97% computed decay versus 96% observed decay from deep to shallow water (averaged over the three lowest observed significant wave heights per case).

It may be pointed out that a significant fraction of the differences with the observations is systematic. The computed waves are generally slightly too steep (the computed significant wave height is about 5% too high, and the mean wave period is about 8% too short). These discrepancies may be ascribed to errors in (or absence of) formulations of physical processes, the bathymetry, the driving wind field, the wind- and wave-induced setup, and the current field. Effects of triad wave-wave interactions, wind speed, and residual low-frequency energy were shown to be inadequate to explain the observed discrepancies. Improving the model results in such complex cases will therefore require more theoretical work (e.g., the regeneration of waves in the presence of low-frequency energy), more modelling efforts (e.g., atmospheric boundary layer models for coastal wind fields), and more practical field work (updated, high-resolution measurements of the bathymetry).

Acknowledgments. We were very fortunate to have access to the original data of all cases. We thank John de Ronde, Joska Andorka Gal, Daan Dunsbergen, Miriam van Endt, and their coworkers at the Ministry of Transport, Public Works and Water Management (the Netherlands) for providing us with the data of the Haringvliet and the Friesche Zeegat and for sharing their initial experiences with the SWAN model. We are equally indebted to Hanz Niemeyer and Ralf Kaiser of the Niedersächsisches Landesamt für Ökologie—Forschungsstelle Küste (Germany) for providing us with the data of the Norderneyer Seegat. Our special thanks go to Caroline Gautier and to Bas Les (M.Sc. students at the Delft University of Technology at the time of this study), who prepared the SWAN computations for the Norderneyer Seegat and carried out the hydrodynamic calculations for the Friesche Zeegat, respectively. We thank David Hurdle of ALKYON of the Netherlands for sharing his ideas on wave dissipation in the presence of swell.

References

Andorka Gal, J. H., Verification set Haringvliet—October 14, 1982–October 15, 1982-, *Rep. RIKZ-95.112x*, 13 pp., Minist. of Transp., Public Works and Water Manage., Den Haag, Netherlands, 1995.

Battjes, J. A., and J. P. F. M. Janssen, Energy loss and set-up due to breaking of random waves, in *Proceedings of the 16th International Conference on Coastal Engineering*, pp. 569–587, Am. Soc. of Civ. Eng., New York, 1978.

Booij, N., R. C. Ris, and L. H. Holthuijsen, A third-generation wave model for coastal regions, 1, Model description and validation, *J. Geophys. Res.*, this issue.

Cavalieri, L., and Malanotte-Rizzoli, Wind wave prediction in shallow water: Theory and applications, *J. Geophys. Res.*, *86*, 10,961–10,973, 1981.

Dingemans, M. W., Verification of numerical wave propagation models with field measurements; CREDIZ verification Haringvliet, *Rep. W488*, part 1b, Delft Hydraulics, Delft, Netherlands, 1983.

Dingemans, M. W., Shift in characteristic wave frequency; some spectra in wave basin and in Haringvliet region, *Rep. H 616*, part II, Delft Hydraulics, Delft, Netherlands, 1989.

Dingemans, M. W., *Water Wave Propagation Over Uneven Bottoms, part 1, Linear Wave Propagation, Adv. Ser. Ocean Eng.*, vol. 13, 471 pp., World Sci., River Edge, N. J., 1997.

Donelan, M. A., The effect of swell on the growth of wind waves, *Johns Hopkins APL Tech. Dig.*, *8*(1), 18–23, 1987.

Dunsbergen, D. W., Verification set Friesche Zeegat—October 1, 1992–November 17, 1992-, *Rep. RIKZ-95.035*, Minist. of Transport, Public Works and Water Manage., Den Haag, Netherlands, 1995.

Eldeberky, Y., Nonlinear transformation of wave spectra in the nearshore zone, Ph.D. thesis, 203 pp., Delft Univ. of Technol., Dep. of Civ. Eng., Delft, Netherlands, 1996.

Hasselmann, K., et al., Measurements of wind-wave growth and swell

decay during the Joint North Sea Wave Project (JONSWAP), *Dtsch. Hydrogr. Z. Suppl.*, *12*(A8), 1–95, 1973.

Hasselmann, S., K. Hasselmann, J. H. Allender, and T. P. Barnett, Computations and parameterizations of the linear energy transfer in a gravity wave spectrum, II, Parameterizations of the nonlinear transfer for application in wave models, *J. Phys. Oceanogr.*, *15*, 1378–1391, 1985.

Komen, G. J., S. Hasselmann, and K. Hasselmann, On the existence of a fully developed wind-sea spectrum, *J. Phys. Oceanogr.*, *14*, 1271–1285, 1984.

Komen, G. J., L. Cavaleri, M. Donelan, K. Hasselmann, S. Hasselmann, and P. A. E. M. Janssen, *Dynamics and Modelling of Ocean Waves*, 532 pp., Cambridge Univ. Press, New York, 1994.

Kuik, A. J., G. P. van Vledder, and L. H. Holthuijsen, A method for the routine analysis of pitch-and-roll buoy wave data, *J. Phys. Oceanogr.*, *18*, 1020–1034, 1988.

Les, B. A. J., Flow computations in the Friesche Zeegat (Stromingsberekeningen in het Friesche Zeegat) (in Dutch), M.Sc. thesis, Delft Univ. of Technol., Dep. of Civ. Eng., Delft, Netherlands, 1996.

Madsen, O. S., Y.-K. Poon, and H. C. Graber, Spectral wave attenuation by bottom friction: Theory, in *Proceedings of the 21st International Conference on Coastal Engineering*, pp. 492–504, Am. Soc. of Civ. Eng., New York, 1988.

Nelson, R. C., Design wave heights on very mild slopes: An experimental study, *Civil. Eng. Trans.*, *29*, pp. 157–161, Inst. of Eng. Aust., Barton, 1987.

Romeiser, R., Global validation of the wave model WAM over a 1-year period using Geosat wave height data, *J. Geophys. Res.*, *98*, 4713–4726, 1993.

Stelling, G. S., A. K. Wiersma, and J. B. T. M. Willemse, Practical aspects of accurate tidal computations, *J. Hydrol. Eng.*, *112*(9), 802–817, 1986.

WAMDI Group, The WAM model—A third generation ocean wave prediction model, *J. Phys. Oceanogr.*, *18*, 1775–1810, 1988.

Whitham, G. B., *Linear and Nonlinear Waves*, 636 pp. John Wiley, New York, 1974.

Zambreski, L., A verification study of the global WAM model, December 1987–November 1988, *Tech. Rep. 63*, Eur. Cent. for Medium-Range Weather Forecasts, Reading, England, 1989.

Zambreski, L., An evaluation of two WAM hindcasts for LEWEX, in *Directional Ocean Wave Spectra*, edited by R. C. Beal, pp. 167–172, Johns Hopkins Univ. Press, Baltimore, Md., 1991.

N. Booij and L. H. Holthuijsen (corresponding author), Faculty of Civil Engineering, Delft University of Technology, Stevinweg 1, 2628 CN, Delft, Netherlands. (L.Holthuijsen@ct.tudelft.nl)

R. C. Ris, WL/Delft Hydraulics, Rotterdamseweg 185, 2629 HD, Delft, Netherlands. (Roeland.Ris@wldelft.nl)

(Received June 16, 1997; revised September 10, 1998;
accepted October 12, 1998.)